ORIGINAL ARTICLE

MicroRNA 199b-5p delivery through stable nucleic acid lipid particles (SNALPs) in tumorigenic cell lines

**Pasqualino de Antonellis · Lucia Liguori · Annarita Falanga ·
Marianeve Carotenuto · Veronica Ferrucci · Immacolata Andolfo ·
Federica Marinaro · Immacolata Scognamiglio · Antonella Virgilio ·
Giuseppe De Rosa · Aldo Galeone · Stefania Galdiero · Massimo Zollo**

Abstract MicroRNA (miR)-199b-5p has been shown to regulate Hes-1, a downstream effector of the canonical Notch and noncanonical SHH pathways, whereby it impairs medulloblastoma (MB) cancer stem cells (CSCs) through a decrease in the CD133+/CD15+ cell population. Here, we have developed stable nucleic acid lipid particles (SNALPs) that encapsulate miR-199b-5p. The efficacy of the miR-199b-5p delivery by these SNALPs is demonstrated by significant impairment of Hes-1 levels and CSC markers in a range of different tumorigenic cell lines: colon (HT-29, CaCo-2, and SW480), breast (MDA-MB231T and MCF-7), prostate (PC-3), glioblastoma (U-87), and MB (Daoy, ONS-76, and UW-228). After treatment with SNALP miR-199b-5p, there is also impairment of cell proliferation and no signs of apoptosis, as measured by caspases 3/7 activity and annexin V fluorescence cell sorter analyses. These data strengthen the importance of such carriers for miRNA delivery, which show no cytotoxic effects and provide optimal uptake into cells. Thus, efficient target downregulation in different tumorigenic cell lines will be the basis for future preclinical studies.

Keywords MiR-199b-5p · SNALP · Hes-1 · Cancer stem cells

Abbreviations

CSCs	Cancer stem cells
DODAP	1,2-Dioleyl-3-dimethylammonium propane
MB	Medulloblastoma
miRs	MicroRNAs
MTS	3-(4,5-dimethylthiazol-2-yl)-5-(3-carboxymethoxyphenyl)-2-(4-sulfophenyl)-2H-tetrazolium)
OMe-	*O*-methyl-
PBS	Phosphate-buffered saline
PEG-Cer16	*N*-Palmitoyl-sphingosine-1-succinyl [methoxy (polyethylene glycol)2000]
RISC	RNA-induced silencing complex
RNAi	RNA interference
siRNAs	Small interfering RNAs
SNALPs	Stable nucleic acid lipid particles

Pasqualino de Antonellis and Lucia Liguori contributed equally to this study.

P. de Antonellis · L. Liguori · M. Zollo (✉)
Dipartimento di Medicina Molecolare e Biotecnologie Mediche, "Federico II" University of Naples, Naples, Italy
e-mail: massimo.zollo@unina.it

P. de Antonellis · L. Liguori · M. Carotenuto · V. Ferrucci ·
I. Andolfo · F. Marinaro · M. Zollo
Biotecnologie Avanzate, CEINGE, Naples, Italy

A. Falanga · S. Galdiero
Dipartimento di Farmacia, Federico II University of Naples, Naples, Italy

I. Scognamiglio · G. De Rosa
Dipartimento di Chimica Farmaceutica e Tossicologica, Facoltà di Farmacia, Federico II University of Naples, Naples, Italy

A. Virgilio · A. Galeone
Dipartimento di Chimica delle Sostanze Naturali, Facoltà di Farmacia, Federico II University of Naples, Naples, Italy

Introduction

Discovery of small (20–30-nucleotide) noncoding RNAs that can regulate genome and gene expression can be considered as one of the most significant advances in cancer

🖄 Springer

therapy of the last 20 years. Effects of these small RNAs on gene expression are generally inhibitory, and corresponding regulatory mechanisms have important roles in all biological pathways. These include effects on cell proliferation, apoptosis, migration, and differentiation, and thus also on the functioning of cancer stem cell (CSC) reprogramming and lineage commitment (Heinrich and Dimmeler 2012). Among the main categories of RNA silencing, microRNAs (miRNAs or miRs) are characterized by a double-stranded precursor and are endogenous regulators of genes that control developmental timing (Meister and Tuschl 2004). Primary miRNA transcripts are generated by RNA polymerase II. In the nucleus, the complex containing the RNase III enzyme Drosha cuts the transcript to release the pre-miRNA hairpin, which is then exported to the cytoplasm by exportin 5 (XPO5). Here, DICER, an endoribonuclease, trims the pre-mRNA from the stem–loop to form a double-stranded miRNA:miRNA complex. This double strand enters into an RNA-induced silencing complex (RISC) that includes the miRNA-loaded Argonaut protein (Ago) and GW182, a glycine–tryptophan repeat-containing protein. Only one of the two strands is stably associated with the Ago effector protein (Fabian and Sonenberg 2012).

Mature miRNA duplexes are short lived, as they are rapidly unwound when they associate with an Ago protein. MiRNA unwinding is accompanied by differential strand retention; one strand is retained while the other strand is lost. The miRNA acts as an adaptor for miRISC to specifically recognize and regulate particular mRNAs. With few exceptions, miRNA-binding sites in animal mRNAs lie in the 3′-UTR, and they are usually present in multiple copies. The degree of miRNA–mRNA complementarity is considered to be the key determinant of the regulatory mechanism. This allows Ago-catalyzed cleavage of the mRNA strand, whereas central mismatches exclude cleavage and promote repression of mRNA translation. It is believed that perfect complementarity excludes translational repression, as it enables cleavage.

Deregulation of miRNA expression has been shown in many tumors and in their corresponding cell lines, as compared to the normal tissues and cells (Calin and Croce 2006; Gaur et al. 2007). The first evidence of the involvement of miRNAs in human cancer is derived from studies on chronic lymphocytic leukemia (CLL). Chromosome 13q14 is deleted in over 65 % of CLL patients, and it contains two miRNA genes, *miR-15a* and *miR-16-1*. There is, thus, the loss of these miRNA activities in patients who have deletion of this region (Calin et al. 2002). Several review articles on the roles of miRNAs in human cancers have been published (Calin et al. 2005; Esquela-Kerscher and Slack 2006; Garzon et al. 2009).

Understanding how the expression levels of miRNAs are finely tuned within a tumorigenic cell and how their gene target regulation occurs in such a complex of multifunctional proteins is now under widespread investigation in cancers

(Kim and Nam 2006; Nana-Sinkam and Croce 2011). Different mechanisms of action have been proposed for the control of their full processing, including genetic, epigenetic, and transcriptional regulation mechanisms (Gaur et al. 2007; He et al. 2007). MiRNAs can function both as oncogenes, which are known as "oncomirs," and as tumor suppressors.

Oncomirs are significantly upregulated in different cancers and can promote tumor development by inhibition of tumor suppressors or of genes that control differentiation or apoptosis (Zhang et al. 2007). Instead, miRNA suppressors can impair tumor growth, invasion and metastasis formation, and CSC dynamism. The miRNAs involved in CSC maintenance have multiple functions, as their gene targets are involved in different cellular pathways, e.g., Wnt, Notch, and SHH (Brennecke et al. 2005; de Antonellis et al. 2011; Zhao et al. 2011; Andolfo et al. 2012; Schoof et al. 2012).

We previously identified miRNA 199b-5p (miR-199b-5p), which acts as a tumorigenesis suppressor in medulloblastoma (MB; a childhood brain tumor), by targeting Hes-1, and we demonstrated miR-199b-5p deregulation in MB. Recently, other targets of miR-199b-5p have been identified: PODXL, DDR1, and HIF-1α (see Garzia et al. 2009; Wang et al. 2011). In acute myeloid leukemia, decreased miR-199b-5p leads to upregulation of PODXL-1 and DDR1, which enhances the proliferation rate of leukemic stem cells and accelerates cell migration and invasion (Favreau et al. 2012).

In MB, we demonstrated that miR-199b-5p can impair the CSC compartment by reducing CD133-positive and CD15-positive cells via Hes-1 downregulation (Garzia et al. 2009). Of note, Hes-1 is a target of the canonical Notch pathway and the noncanonical SHH and Wnt pathways (Morton and Lewis 2007; Ingram et al. 2008; Shimizu et al. 2008). A crucial role for the Notch target gene *Hes-1* was emphasized by Schreck et al., who demonstrated Hes-1 binding to the Gli1 first intron and defined its mechanism of regulation (Schreck et al. 2010). Moreover, in a recent phase I trial, Fouladi et al. estimated the maximum tolerated dose of MK-0752 and characterized its pharmacokinetic properties as a γ-secretase (Notch/Hes-1 pathway) inhibitor in children with refractory or recurrent central nervous system malignancies, such as glioma, ependymoma, and MB (Fouladi et al. 2011). Indeed, Hes-1 is also regulated by the SHH pathway, through a mechanism that does not involve γ-secretase-mediated Notch cleavage and that probably involves transcription factors other than RBP-Jk in MB (Morton and Lewis 2007).

It is well known that the Notch pathway has a crucial role in embryogenesis, tissue patterning, and morphogenesis and its dysfunction can occur in a wide range of tumors, from hematological cancers, such as leukemia and lymphoma, to solid tumors, such as colon, prostate, and brain tumors (Fouladi et al. 2011; Bertrand et al. 2012; Danza et al.

2012; Gursel et al. 2012). Many studies have highlighted the activation of the Notch pathway in colon cancer, and in particular, Hes-1 expression was shown to be higher in primary tumors than in distant metastases (Katoh and Katoh 2007; Reedijk et al. 2008). In breast cancer, instead, Mittal et al. showed high expression of Hes-1 in almost 75 % of breast cancers analyzed (Mittal et al. 2009).

Gene silencing by RNA interference (RNAi) has become the optimal method for target gene identification and validation (Dorsett and Tuschl 2004). In mammalian cells, it has been reported that siRNA actions remain effective only for an average of ca. 66 h (Chiu and Rana 2002) because of poor nuclease resistance and the unfavorable metabolic and thermal stability arising from their short oligoribonucleotide sequences (Bumcrot et al. 2006). In addition, it has been shown that siRNAs induce an innate immune stimulation in vivo, with high levels of inflammatory cytokines, such as tumor necrosis factor-α, interleukin-6, and interferon-α, with effects on the regulation of gene expression (Robbins et al. 2009). To improve the nuclease resistance and thermal stability of siRNAs, several chemical modifications to their sugar and phosphate backbone have been attempted (Watts et al. 2008). In particular, 2′-O-methyl (2′-OMe) modifications have provided increases in stability that correlate to the number of substitutions (Czauderna et al. 2003), thus preventing the innate immune responses indicated above (Judge et al. 2006).

Despite such modifications that can increase the effectiveness of RNAi, the therapeutic potential of miRNAs is hampered by other drawbacks, such as poor cell uptake and degradation in the lysosomal compartments (Whitehead et al. 2009). The use of viral carriers allows high transfection efficiency to be achieved, although this approach is very expensive and can be dangerous due to immunogenicity and possible viral reactivation. Conversely, nonviral carriers are relatively cheap, safe, and easy to manipulate, as compared to viral carriers. Many different types of nonviral carriers have been developed to provide solutions to successful tumor targeting of siRNAs. Lipid-based nanoparticles are now, by far, the most widely used and studied nanocarriers for cancer therapy (Moreira et al. 2008). Among various lipid-based formulations, a classical example is the use of "liposomes", while an emerging novel class are the so-called solid lipid nanoparticles or nanostructure lipid carriers (Puri et al. 2009). Of note, recent preclinical studies using biocompatible polymers, such as poly-lactic-co-glycolic acid carrying miRNA-155, together with the use of a "penetratin" peptide, have shown therapeutic benefit in a lymphoma animal model (Babar et al. 2011). Most recently, nanoparticle-sized issues are under investigation because of their efficacy for internalization in eukaryotic cells. Martins et al. showed that different tumorigenic cell lines (glioma and macrophage) can internalize lipid nanoparticles with mean diameter <200 nm and with a slightly negative surface charge (−20 mV) (Martins et al. 2012).

For the delivery of nucleic acids, including siRNAs, cationic liposomes have been the most extensively used (Moreira et al. 2008). Complexing of cationic liposomes with negatively charged siRNAs generates lipoplexes with high efficacy for mediation of siRNA transfection (Simoes et al. 2005). For use in vivo, where it is necessary to provide protection from blood nucleases and to extend their blood circulation, these cationic liposomes have been protected with hydrophilic molecules, such as poly(ethyleneglycol) (PEG) (Gomes-da-Silva et al. 2012). The most notable of the PEG formulations are the "stable nucleic acid lipid particles" or SNALPs (Morrissey et al. 2005; Judge et al. 2009). SNALPs have been successfully used to aid in the silencing of therapeutically relevant genes in rodents and in nonhuman primates (Zimmermann et al. 2006; Frank-Kamenetsky et al. 2008). Morrissey et al. described the efficacies of SNALPs (with a size of 140± 12 nm) that encapsulate siRNAs targeted to HBV RNA in a mouse model of HBV replication. Here, they showed a longer half-life in plasma and liver and reduced toxic and immunostimulatory side effects (Morrissey et al. 2005). Yang et al. instead described cationic lipid-assisted polymeric nanoparticles of (poly(ethylene glycol)-b-poly(d,l-lactide) at around 170 to 200 nm in size, which were used to suppress tumor growth in an MDA-MB-435 murine xenograft model and which suggested therapeutic promise in disease treatment (Yang et al. 2011). Additional improvements have shown significant efficacy in vivo, with the development of new cationic lipids in formulations to deliver siRNAs in rodents and nonhuman primates (Semple et al. 2010). These have used 1,2-dilinoleyloxy-3-dimethylaminopropane substituted with new molecules, such as 2,2-dilinoleyl-4-(2-dimethyl aminoethyl)-[1,3]-dioxolane.

Due to the previous data obtained in MB with miR-199b-5p and to the deregulation of the Notch pathway in several tumor types, we investigated the development of a SNALP formulation to deliver miR-199b-5p into different cancer cell lines in vitro. Thus, we prepared and characterized SNALPs that can encapsulate the mature 2′-O-methylated (2′-OMe)-miR-199b-5p. This formulation was investigated in a range of different human cancer cell lines (colon, breast, prostate, and brain) to define the SNALP encapsulation of miR-199b-5p and their combined actions, which are mainly through Hes-1 inhibition.

Materials and methods

Lipids and chemicals

1,2-Dioleyl-3-dimethylammonium propane (DODAP) and N-palmitoyl-sphingosine-1-succinyl [methoxy(polyethylene glycol)2000] (PEG-Cer16) were purchased from Avanti Polar Lipids. Disteroylphosphatidylcholine (DSPC) was

kindly donated by Lipoid GmbH (Cam, Switzerland). Cholesterol, sodium chloride, potassium chloride, sodium phosphate, HEPES, citric acid, and sodium citrate were purchased from Sigma-Aldrich (Milan, Italy). Ethanol and other reagents were obtained from Carlo Erba Reagenti (Milan, Italy).

2′-OMe–oligonucleotide synthesis and purification

The 2′-OMe–oligonucleotides were synthesized on a Millipore Cyclone Plus DNA synthesizer at a 1 μmol scale using commercially available 5′-O-(4,4′-dimethoxytrityl)-2′-OMe-3′-O-(2-cyanoethyl-N,N-diisopropyl) RNA phosphoramidite monomers and 2′-OMe RNA SynBase CPG 1000/110 as the solid-phase support (Link Technologies). The sequence of the mature miR-199b-5p (2′-OMe is inserted into each following nucleotide) is: 5′-C C C A G U G U U U A G A C U A U C U G U U C - 3′ (MIMAT0000263, miRBase 18 released; www.mirbase.org) and its scrambled control (2′-OMe in each base) was: 5′-GGUUGUAUGCAUUCCCUAUCUAC-3′. The oligomers were detached from the support and deprotected by treatment with concentrated aqueous ammonia for 12 h at 55 °C. The combined filtrates and washings were concentrated under reduced pressure, dissolved in H_2O, and analyzed and purified by anion exchange high-performance liquid chromatography on a NUCLEOGEL SAX column (Macherey-Nagel, 1000-8/46) using buffer A: 20 mM KH_2PO_4/K_2HPO_4 aqueous solution (pH 7.0), containing 20 % (v/v) CH_3CN; and buffer B: 1 M KCl, 20 mM KH_2PO_4/K_2HPO_4 aqueous solution (pH 7.0), containing 20 % (v/v) CH_3CN. These were used as a linear gradient from 0 % B to 100 % B over 45 min at a flow rate of 1 ml/min. The purified oligomers were successively desalted using Sep-Pak C18 cartridges (Waters) and characterized by electroionization mass spectrometry.

Preparation and characterization of stable nucleic acid lipid particles

Lipid stock solutions were prepared in ethanol. Typically, 6.5 μmol total lipid (0.2 ml total volume) was added to a glass tube. In a separated tube, 1 mg miRNA was dissolved in 0.3 ml 20 mM citric acid, pH 4.0. The two solutions were warmed for 2–3 min at 65 °C, and the lipid solution was quickly added to the miRNA solution while stirring. The mixture was passed 30 times through three-stacked 100-nm polycarbonate filters using a thermobarrel extruder (Northern Lipids Inc., Vancouver, BC, Canada) maintained at approximately 65 °C. Nonencapsulated miRNA was removed by chromatography using a Sephadex G-50 DNA grade column (GE Healthcare, Milan, Italy). A typical 0.5 ml formulation contained 6.5 μmol DSPC/cholesterol/DODAP/PEG-Cer16 (25 mol/45 mol/20 mol/10 mol) and 1 mg miRNA. The

encapsulation efficiency was about 80 %. The mean diameter and size distribution of the SNALPs were determined at 37 °C by Nano-Zs (Malvern, UK). Each sample was diluted in phosphate-buffered saline (PBS), filtered with 0.22-μm pore size polycarbonate filters (MF-Millipore, Microglass Heim, Naples, Italy), and analyzed with the detector angle at 173°. The polydispersity index was measured to determine the particle size distribution. For each batch, the diameter and size distributions were calculated as the means of three measures. For each formulation, the diameter and polydispersity index were calculated as the means of two different batches. The 1 μmol of miRNA encapsulated in the SNALPs were measured spectrophotometrically. Briefly, 2 μl SNALP suspension was analyzed at 260 nm using a nanoprobe (Thema Research, Bologna, Italy), and the encapsulation efficiencies were calculated as the ratio of the initial and final oligodeoxynucleotide-to-lipid ratios (×100).

Cell culture

Different cell lines were used in this study: three derived from colon cancers (HT-29 cells, code ATCC #HTB-38, Manassas, VA, USA; CaCo-2 and SW480 cells from the Culture Tissues Facility, CEINGE, Naples, Italy), two from breast cancers (MDA-MB231T cells, ATCC code HTB-26, Manassas, VA, USA; MCF-7 cells, from the Culture Tissues Facility, CEINGE, Naples, Italy), one from prostate cancer (PC-3 cells, code PC-3 M, Caliper, Paris, France), one from glioblastoma (U-87 cells, code U-87 MG, Caliper, Paris, France), and three from MB (Daoy, UW-228 and ONS-76, ATCC #HTB-186, #14963, and # HTB-182, respectively, Manassas, VA, USA). The HT-29 and MDA-MB231T cells were cultured in Dulbecco's modified Eagle's medium (DMEM) (EuroClone, Pero, Italy); the Daoy, UW-228, U-87, PC-3, and MCF-7 cells were cultured in minimum essential Eagle's medium (M5650; Sigma-Aldrich, Milan, Italy); and the SW480 and ONS-76 cells were cultured in RPMI 1640 (EuroClone, Pero, Italy). All of the media were supplemented with 10 % fetal bovine serum, 2.0 mM L-glutamine, 1.0 mM sodium pyruvate, 100 μg/ml streptomycin, and 100 U/ml penicillin G, with the cells kept at 37 °C in a 5 % CO_2 and 95 % air humidified atmosphere. The cell lines were grown in 10-cm plates.

Transient transfection and luciferase assay

Human embryonic kidney (HEK-293T) cells were cultured in DMEM containing 10 % fetal bovine serum, 2.0 mM L-glutamine, and 1 % penicillin/streptomycin in a humidified atmosphere with 5 % CO_2. For transfection, the HEK-293T cells were plated and incubated overnight at 37 °C. The following day, immediately prior to transfection, their medium was changed. The transfections were carried out using

calcium phosphate according to the standard protocol. When at 60 % confluence, the HEK-293T cells were transfected with 15 μg DNA per 10-cm dish using vectors encoding the Hes-1 3′-UTR (TK-Renilla Hes-1). After 12 h, the SNALP miR-199b-5p and SNALP with the scrambled miRNA (SNALP scramble) were added. The following day, the medium was changed, and reporter assays were performed after 48 h and 72 h using the Dual-Luciferase® Assay reporter system (Promega, Madison, WI, USA) according to the manufacturer instructions.

Treatment of cell lines with the SNALPs

The HT-29, CaCo-2, SW480, MCF-7, PC-3, U-87, ONS-76, Daoy, UW-228, and MDA-MB231T cells were seeded in duplicate into six-well plates at a density of 2.5×10^5 cells/well. After their attachment, they were treated with medium without serum but containing the SNALPs (25 μg/ml or 50 μg/ml miR-199b-5p oligonucleotide, as the standard miRNA concentrations throughout the study) for 8 h at 37 °C in a 5 % CO_2 incubator. After this time, the medium was replaced with medium containing fetal bovine serum for the following 72 h and then the cells were pelleted for further analyses.

Proliferation assay

Cell proliferation was determined using CellTiter96 AQueous Nonradioactive Cell Proliferation Assay kits (Promega Madison, WI, USA). The HT-29, MDA-MB231T, Daoy, and UW-228 cells were seeded into 96-well plates at a density of 3×10^3 cells/well in complete DMEM or minimum essential Eagle's medium, with SNALP miR-199b-5p and SNALP scramble at a final concentration of 50 μg/ml. After 24, 48, and 72 h, 3-(4,5-dimethylthiazol-2-yl)-5-(3-carboxymethoxyphenyl)-2-(4-sulfophenyl)-2H-tetrazolium) (MTS) was added to each well, and after 2 h, the absorbance of each well was measured at 490 nm using a VICTOR3 Multilabel counter (PerkinElmer, Monza, Italy). Each experiment was performed with five replicates (wells) and was repeated twice.

Cell index proliferation assay

The cell index (CI) was derived as the relative change in the measured electrical impedance, as representative of the cell status. This assay allows label-free dynamic monitoring of cell proliferation and viability in real-time. The CaCo-2, SW480, MCF-7, PC-3, U-87, and ONS-76 cells were seeded at 5,000 cells/well into 100 μl complete medium in 96-well microtiter plates (E-plates). The attachment, spreading, and proliferation of the cells were monitored every 30 min using the RT-CES® system (xCELLigence by Roche).

Approximately 24 h after seeding and after 3 h of starvation, the cells were treated with 100 μl SNALP miR-199b-5p and SNALP scramble (50 μg/ml) in medium without serum for 4 h. After this time, 100 μl medium was added to each well, and the cell proliferation was monitored for 24 h to 130 h, depending on experimental design. The CI at each time point was defined as $(R_n - R_b) / 15$, where R_n is the cell electrode impedance of the well when it contained cells, and R_b is the background impedance of the well with medium alone.

RNA isolation, cDNA preparation, and quantitative real-time PCR

Total RNA was extracted from the cell lines using TRIzol reagent (Invitrogen). Synthesis of cDNA from the total RNA (2 μg) was with SuperScript II First-Strand kits (Invitrogen). Quantitative real-time PCR (qRT-PCR) was performed using the SYBR Green method, following standard protocols, with an Applied Biosystems ABI PRISM 7900HT Sequence Detection system. Relative gene expression was calculated using the $2^{(-\Delta Ct)}$ method, where ΔCt indicates the differences in the mean Ct between selected genes and the internal control (Livak and Schmittgen 2001). qRT-PCR primers for each gene were designed using the Primer Express software, version 2.0 (Applied Biosystems). The primer sequences are indicated below: *HES-1* forward, (5′–3′) AATGACAGTGAAGCACCTCCG; *HES-1* reverse, (3′–5′) CACTTGGGTCTGTGCTCAGC; *PODXL-1* forward, (5′–3′) TCAAGCACTGTGGCTATCCCT; *PODXL-1* reverse, (3′–5′) TCAAGCACTGGCTATCCCT; *DDR1* forward, (5′–3′) CTGGATGGGCTGGAAGGA; *DDR1* reverse, (3′–5′) TCCTTCAGCACCACTCCCTC; *HIF-α* forward, (5′–3′) CTCAGTCGACACAGCCTGGA; *HIF-α* reverse, (3′–5′) TTCTTCTGGCTCATATCCCATCA. The significance of the gene expression differences were determined using the Student's t test; statistical significance was established as $p < 0.05$. All statistical analysis was performed using Excel, included in the Office 2007 suite released by Microsoft.

TaqMan miRNA assay

Reverse transcriptase reactions

The reverse transcriptase reactions for miR-199b-5p and mMU6 were performed with 40 ng RNA, 50 nM stem–loop reverse transcriptase primer, 1× reverse transcriptase buffer (P/N: 4319981, Applied Biosystems, Branchberg, NJ, USA), 0.25 mM of each dNTP, 3.33 U/ml MultiScribe Reverse Transcriptase (P/N: 4319983, Applied Biosystems), and 0.25 U/ml RNase inhibitor (P/N: N8080119; Applied Biosystems). The 15-μl reactions were incubated in an Applied Biosystems

9700 thermocycler for 30 min at 16 °C, 30 min at 42 °C, and 5 min at 85 °C and then held at 4 °C.

Real-time PCR

RT-PCR was performed for all of the cell lines analyzed using a standard TaqMan PCR kit protocol on an Applied Biosystems 7900HT Sequence Detection system. The 20-μl PCRs included 2 μl reverse transcriptase product, 10 μl TaqMan Universal PCR Master Mix (Applied Biosystems), and 0.2 mM TaqMan probe (Applied Biosystems: MiR-miR-199b-5p: identification number 00500, code 4427975; MU6: identification number 001093, code 4427975). The reactions were incubated in 96-well plates at 95 °C for 10 min, followed by 60 cycles of 95 °C for 15 s, and 60 °C for 1 min.

Western blotting

Western blotting was performed on the total protein extracts of the human cancer cell lines for the HT-29, CaCo-2, SW480, MDA-MB231T, MCF-7, PC-3, U-87, ONS-76, Daoy, and UW-228 cells after 72 h of treatment. For the total protein fraction, the harvested cells were washed three times with ice-cold PBS and lysed in RIPA buffer. Protein concentrations in cell extracts were determined using the Bradford assay (BioRad, Milan, Italy). Fifty microgram total lysates was loaded onto 12 % polyacrilamide gels and then transferred to nitrocellulose membranes. The membranes were blocked with 5 % nonfat milk in PBS, pH 7.6, 0.02 % Tween 20 for 1 h and then incubated with the relevant polyclonal antibody: anti-Hes-1 (1:200; sc 25392; Santa Cruz Biotechnology), anti-CD15 (1:250; sc 53290; Santa Cruz Biotechnology), anti-CD133 (1:250; ab 16518; Abcam), and anti-CD44 (1 μg/ml; ab 41478; Abcam). After washing in PBS, pH 7.6, 0.02 % Tween 20, the membranes were incubated with a horseradish peroxidase-conjugated goat anti-rabbit antibody (1:3,000) and a horseradish peroxidase-conjugated goat anti-mouse antibody (1:5,000; Santa Cruz Biotechnology, Santa Cruz, CA, USA). The immunoblots were visualized using ECL detection kits, with enhanced chemiluminescence (Pierce, Rockford, IL, USA). A mouse β-actin antibody (1:1,000; Sigma-Aldrich, Milan, Italy) was used as the control for equal loading of total lysates.

Results

Characteristics of SNALP miR-199b-5p

The methodology for SNALP production used here was through "membrane extrusion," in contrast to the "high-pressure homogenization" methodology that is usually used in industrial production to obtain reliable and homogeneous populations of nanoparticles (with a size range <100 nm). For this reason, the SNALPs developed here were in a range of sizes >100 nm; nevertheless, Martins et al. showed that such particles can internalize in cells in vitro, as for those used in solid lipid nanoparticle formulations (Jores et al. 2005; Martins et al. 2012). The SNALPs containing miR-199b-5p were characterized by measuring their size, surface properties, and miR-199b-5p oligonucleotide loading. Here, we encapsulated the mature single-strand miR-199b-5p in the SNALP molecules to study its biological effects in different cell lines. As is known, RNAi, as a single-strand status, is less resistant than siRNA duplexes. We used the 2′-OMe modification for each of the following nucleotides to impair nuclease degradation and to improve miR-199b-5p thermal stability. The characteristics of the SNALP miR-199b-5p are reported in Table 1. The SNALPs with the scrambled miRNA (SNALP scramble) included two populations, one at ca. 199.6 nm in size and the second at ca. 78.4 nm; the SNALP miR-199b-5p, instead, showed two main population peaks: the first at ca. 258.8 nm and the second at ca. 84.7 nm (see Table 1). Our SNALP production had a polydispersivity index (PI) of ca. 0.2. The negative zeta potential showed the absence of a net positive charge on the SNALP surface. Finally, the miR-199b-5p encapsulation efficiency was measured as close to 80 %.

SNALP miR-199b-5p binds to the 3′-UTR of Hes-1

In our previous study, we demonstrated that miR-199b-5p binds to the 3′-UTR of its predicted target gene Hes-1 and significantly impairs Hes-1 expression (Garzia et al. 2009). Thus, one of the major initial questions raised here was whether miR-199b-5p encapsulated in the SNALPs has these same effects in terms of its target recognition. For this purpose, we used a Renilla luciferase reporter that contained the 3′-UTR of the human Hes-1 mRNA downstream of the Renilla luciferase coding region, the expression of which was driven by the thymidine kinase (Tk) promoter (Supplementary Fig. 1a). The reporter construct (Tk-ren/Hes-1) and the SNALP miR-199b-5p were transfected into HEK-293T cells over 48 h and 72 h, with the pGL3-CMV-firefly vector to normalize for transfection efficiency. Two different concentrations of SNALP miR-199b-5p and SNALP scramble were used: 25 μg/ml and 50 μg/ml. The experiments carried out with 25 μg/ml SNALP miR-199b-5p had no significant effects on luciferase activity (data not shown). Interestingly, the relative luciferase activity was markedly decreased in cells transfected with the Tk-ren/Hes-1 construct and treated with SNALP miR-199b-5p (50 μg/ml), compared to SNALP scramble. The values of luciferin activity observed were significantly higher at 72 h (by ca. 60 %) than at 48 h ($p=0.02$; Supplementary Fig. 1a). No variations were measured for the relative luciferase activity assays within the treated HEK-293 T cells with either empty SNALPs or

Table 1 Structural characteristics of the SNALP miR-199b-5p and scramble liposome formulations

Formulation	Mean diameter peak 1 (nm ± SD)	% volume peak 1	Mean diameter peak 2 (nm ± SD)	% volume peak 2	Polydispersity index ± SD	Zeta potential (mV ± SD)
SNALP miR-199b-5p						
Batch 1	250.0±6.84	57.7	70.64±4.42	42.3	0.267±0.001	−5.09±0.11
Batch 2	258.8±7.72	55.3	84.66±2.92	44.7	0.257±0.001	−7.03±0.19
SNALP scramble						
Batch 1	194.0±5.08	84.5	72.38±3.02	15.5	0.175±0.006	−10.71±0.34
Batch 2	199.6±4.47	87.4	78.46±2.46	12.5	0.135±0.008	−14.49±0.31

Zeta potential, size, and percentage in volume of liposome formulation are expressed as *z*-average, as measured by DSL and polydispersivity index. Data are expressed as means±standard deviation (SD) of three separate experiments for each of two batch formulations, with at least 13 measurements for each

SNALP scramble (Supplementary Fig. 1a). One explanation for this negative downregulation of Hes-1 using 25 μg/ml SNALP miR-199b-5p would be due to the presence of the two different size populations of the SNALP nanoparticles (as shown in Table 1). Here, we measured two peaks of particle elution, with size ranges between 70–84 nm (as 44 % of the SNALP population) and 250–258 nm (as 57 % of the SNALP population). The data obtained with the scrambled miRNA-containing SNALPs (SNALP scramble) showed similar size values of the second peak, which ranged from 72 to 78 nm, with a substantial difference in the volume (reduced to 14 %, on average). Overall, our data are in agreement with literature reports that have shown that this second peak population (<100 nm in size) can enter eukaryotic cells more efficiently than other population sizes. Thus, at this time, we can assume that the SNALPs with the smaller diameters (<100 nm) can carry the miR-199b-5p into tumorigenic cells with good internalization and with binding to the 3′-UTR of *Hes-1* mRNA, which showed reduced expression and protein synthesis.

Delivery of miR-199b-5p by SNALPs compared to "naked" oligonucleotide

To investigate the efficiency of miR-199b-5p delivery by the SNALPs as compared to the "naked" miR-199b-5p oligonucleotide (not encapsulated in SNALPs), we treated HT-29 colon cancer cells for 72 h, according to previously obtained luciferase assay data. At this time, we performed TaqMan RT-PCR assays to compare the expression of miR-199b-5p in the HT-29 cells after these two different treatments. As shown in Supplementary Fig. 1c, the expression of miR-199b-5p did not change in cells treated with the "naked" oligonucleotide, as compared to the untreated cells (which showed the endogenous levels of miR-199b-5p in these HT-29 cells), while the expression of miR-199b-5p was increased after treatment with SNALP miR-199b-5p (Supplementary Fig. 1c). Hes-1 expression was further tested in cells treated with the "naked" miR-199b-5p,

confirming that it cannot enter the cells to downregulate Hes-1 expression (Supplementary Fig. 1c).

Impaired proliferation rates by SNALP miR-199b-5p in different tumorigenic cell lines

We have previously demonstrated that miR-199b-5p impairs cell proliferation in MB cell stable clones overexpressing miR-199b-5p, thus showing that this phenomenon is directly correlated with Hes-1 downregulation (Garzia et al. 2009). Here, to determine whether SNALP miR-199b-5p delivery has similar biologic effects in different cell lines, we performed proliferation assays. We initially treated HT-29 cells with 25 μg/ml SNALP miR-199b-5p and SNALP scramble for up to 72 h. The efficiency of the delivery of the SNALPs was monitored through analysis of miR-199b-5p expression using the TaqMan RT-PCR assay. As shown in Supplementary Fig. 1b, at 72 h, there was significant overexpression of miR-199b-5p in cells treated with SNALP miR-199b-5p (to ca. fivefold the control). The cell proliferation rate, which was determined using MTS (see "Materials and methods"), and the Hes-1 protein expression were not impaired at this concentration of SNALP miR-199b-5p (Supplementary Fig. 1b). These data are similar to those obtained in the HT-29 cell line with the luciferase assay, where 25 μg/ml SNALP miR-199b-5p had no effects on Hes-1 downregulation and impairment of the cell proliferation rate.

To set up the optimal conditions for our SNALP miR-199b-5p treatments, we tested a time course of sampling at 3, 6, 9, 12, 24, and 72 h using 50 μg/ml SNALP miR-199b-5p and SNALP scramble, following the effects on Hes-1 expression in HT-29 cells by Western blotting (Supplementary Fig. 1d, e). Indeed, here, we observed that miR-199b-5p expression gradually increased (at 6 and 12 h), although at the early time points (3, 6, 9, 12, and 24 h), there were no significant changes in the cell proliferation rate and Hes-1 protein expression. For these reasons,
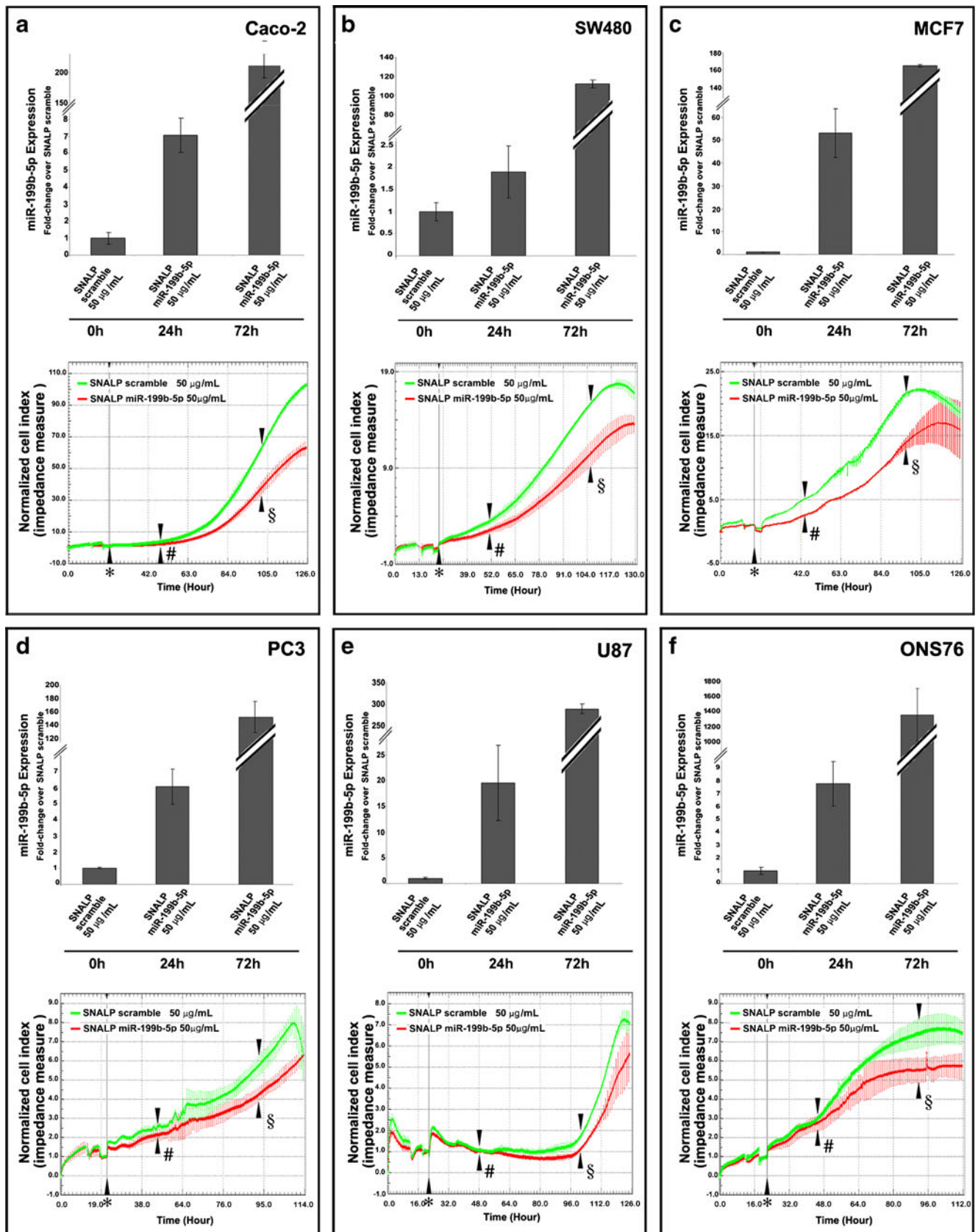
◀ **Fig. 1** MiR-199b-5p delivery by SNALPs, and impairment of proliferation rates in different cell lines. *Top* for each tumorigenic cell line analyzed (colon cancer CaCo-2 and SW480 cells, breast cancer MCF-7 cells, prostate cancer PC-3 cells, glioblastoma U-87 cells, and MB ONS-76 cells), the *histograms* indicate the miR-199b-5p expression after treatment with SNALP miRNA 199b-5p and SNALP scramble, using TaqMan PCR assays. The *Y*-axis indicates miRNA 199b-5p expression as fold changes over SNALP scramble, and the *X*-axis indicates the analysis times (h). *Bottom* Cell index assays as a measure for cell proliferation of the tumorigenic cell lines after the same treatments. The *Y*-axis indicates the impedance (proportional to cell numbers) and the *X*-axis indicates the analysis times (h). *Green line* treatment with SNALP scramble, *red line* treatment with SNALP miR-199b-5p. *Symbols* (*below the red and green curves*) indicate the times of SNALP administration to cells: *asterisks* (*below the X-axis*) are indicating the time of added medium with fetal bovine serum in the plates, *number sign* 24 h after treatment, *section sign* 72 h after treatment

we used the HT-29 cells for SNALP miR-199b-5p treatments of 72 h, with 50 μg/ml SNALP miR-199b-5p and SNALP scramble. At this treatment time, we measured the expression of miR-199b-5p using TaqMan RT-PCR assays. As shown in Supplementary Fig. 2a, the levels of miR-199b-5p were significantly higher in cells treated with 50 μg/ml SNALP miR-199b-5p ($p = 0.008$), as compared to those treated with 50 μg/ml SNALP scramble. Also, the proliferation rate of these HT-29 cells, as determined using the MTS assay (see "Materials and methods"), was significantly impaired at the same SNALP miR-199b-5p concentration ($p = 0.03$), as shown in Supplementary Fig. 2a (data presented for the HT-29, Daoy, UW-228, and MDA-MB-231T cells). According to the luciferase assays, our data demonstrate that miR-199b-5p delivery by SNALPs (at 50 μg/ml) was efficient in these HT-29 cells at 72 h post-treatment and that after this time, there was significant impairment of cell proliferation due to the overexpression of miR-199b-5p.

Efficiency of SNALP miR-199b-5p delivery and impairment of proliferation in different cell lines

To further address the ubiquitous delivery of these SNALPs in several tumorigenic cell lines, we investigated other cellular models for the efficiency of SNALP delivery of miR-199b-5p. For this, we treated several cell lines from different tumor types with 50 μg/ml SNALP miR-199b-5p, and through TaqMan RT-PCR assays, this revealed the expression of miR-199b-5p after 72 h of treatment. CaCo, SW480, MCF-7, PC-3, U-87, ONS-76, Daoy, UW-228, and MDA-MB231T cells were used here. As shown in Fig. 1, by measuring the mRNA levels of exogenous miR199-b-5p in all of these cell lines analyzed, we saw that internalization of miR-199b-5p was already achieved at 24 h of treatment, although at 72 h the fold changes observed were significantly greater. Moreover, after the same treatment with SNALP miR-199b-5p (50 μg/ml) for 72 h, we observed a different

efficacy of miR-199b-5p internalization, potentially due to the different lipid compositions of the cell membranes of these different cell types and to their levels of endocytosis. These are artifacts that can infer differences in the intracellular acquisition of these particles according to the specific cell membrane structure and composition. At 72 h, we measured the optimum internalization of these SNALPs in the ONS-76 cells ($p = 0.003$) (Fig. 1f), followed by the CaCo-2 ($p = 0.004$) (Fig. 1a), SW480 ($p = 0.0007$) (Fig. 1b), MCF-7 ($p = <0.0001$) (Fig. 1c), U-87 ($p = 0.0008$) (Fig. 1e), PC-3 ($p = 0.012$) (Fig. 1d), and MDA-MB231T ($p = 0.0002$) (Supplementary Fig. 2a) cells. Lower levels of internalization were measured in the Daoy ($p = 0.150$) and UW-228 ($p = 0.001$) cells, as shown in Supplementary Fig. 2a. The histogram in Supplementary Fig. 2b shows the levels of miR-199b-5p expression after this treatment in all of the cell lines (for $2^{\Delta Ct}$ values see Supplementary Table 2).

To confirm the previous data on the impairment of cell proliferation, as obtained in HT-29 cells, we performed CI analyses or MTS assays in all of these cell lines, with the analysis by TaqMan RT-PCR. Thus, to monitor the effects of SNALP miR-199b-5p on cell proliferation in real-time, we used the CI assay with the CaCo-2, SW480, MCF-7, PC-3, U-87, and ONS-76 cells (for impedance values, see Supplementary Table 1). As shown in Fig. 1, 50 μg/ml SNALP miR-199b-5p significantly impaired the proliferation of all of these treated cells, with greater effects around 72 h (CI *p* values <0.0001 for all tumorigenic cells treated), in agreement with the TaqMan RT-PCR for miR-199b-5p expression in the same cell lines. After 72 h, we observed no significant variations, and we speculate that this is due to the time of the intracellular stability of 2′-OMe-miR-199b-5p. Indeed, as shown by Takahashi et al. (2012), although the 2′-OMe modification appears to be valid for the duration of oligonucleotide stability in cells and for its interference activity, after 72 h, 2′-O-Me siRNAs show drastic reductions in their activities. Finally, to confirm the impairment of proliferation also in other cell lines, we used an additional method to measure cell proliferation, the classical MTS assay, in Daoy ($p = 0.03$), UW-228 ($p = 0.05$), and MDA-MB231T ($p = 0.003$) cells. As shown in Supplementary Fig. 2a, although the rate of internalization of SNALP miR-199b-5p was significantly lower compared to the other cell lines investigated here, the cell proliferation rates were still impaired in these cells.

SNALP miR-199b-5p treatment of several cancer cell lines leads to impairment of Hes-1 mRNA and protein expression

To see if the biological effects on cell proliferation directly influence the downregulation of the miR-199b-5p target, we analyzed the levels of *Hes-1* mRNA and the Hes-1 protein in all of the cell lines investigated here. First, we performed
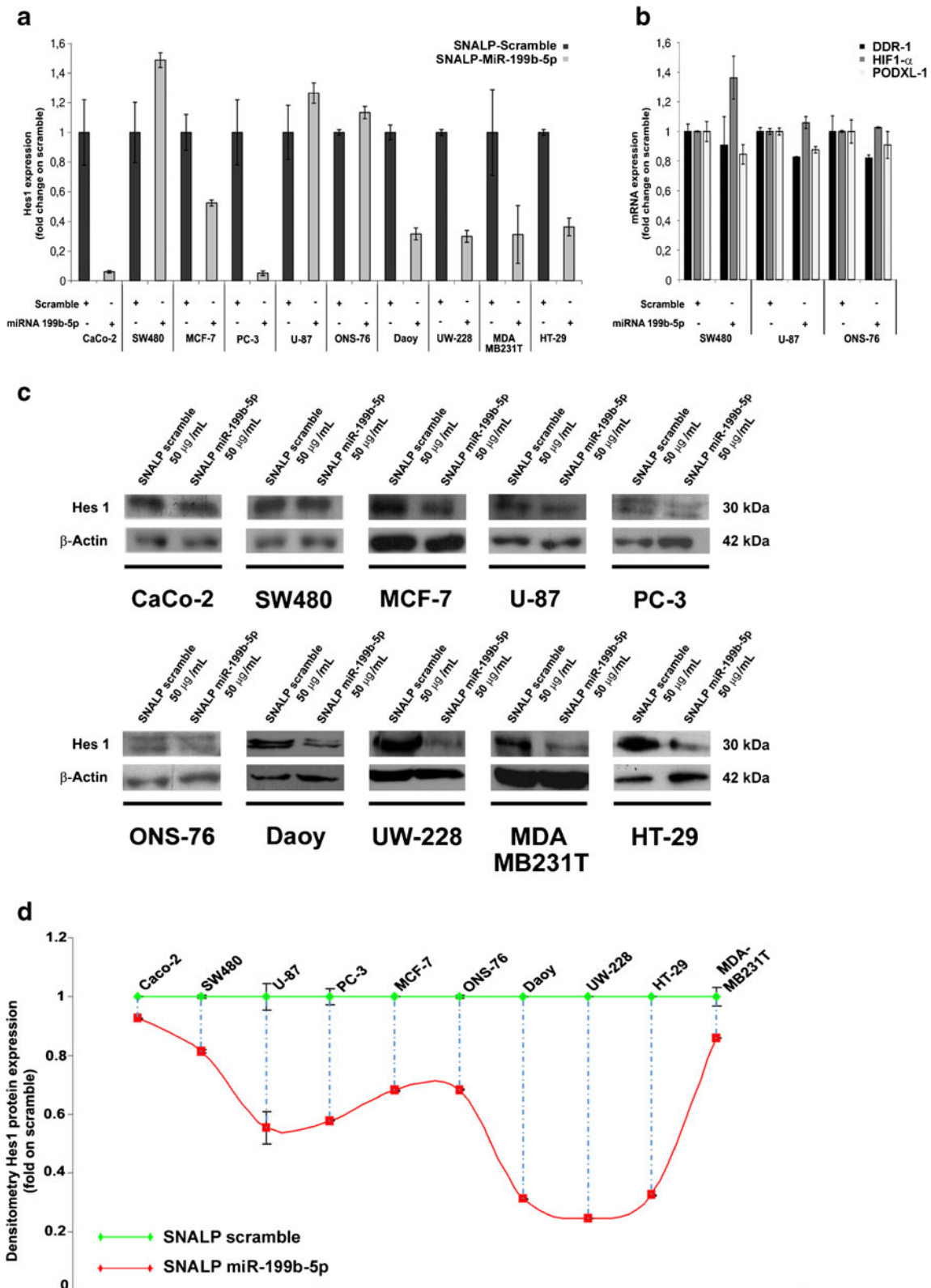
Western blotting to determine the basal levels of the Hes-1 protein, and as shown in Supplementary Fig. 2c, we found different endogenous expression of the Hes-1 protein across these different cell lines. It should be noted here that the Hes-1 endogenous protein was revealed using polyclonal antibodies, which showed a nonspecific protein band (the

◀ **Fig. 2** Downregulation of *Hes-1* mRNA, the Hes-1 protein, and *DDR1*, *PODXL-1*, and *Hif-1α* mRNAs in several cancer cell lines after treatment with SNALP miR-199b-5p. **a** Downregulation of *Hes-1* mRNA expression analyzed by Syber qRT-PCR after 72-h treatment with SNALP miR-199b-5p and SNALP scramble in colon cancer CaCo-2 and HT-29 cells, breast cancer MCF-7 and MDA-MB231T cells, prostate cancer PC-3 cells, and MB ONS-76, Daoy and UW-228 cells. **b** Variations in *DDR1*, *PODXL-1*, and *Hif-1α* mRNA expression analyzed by Syber qRT-PCR after 72 h of treatment with SNALP miR-199b-5p and SNALP scramble in colon cancer SW480, MB ONS-76, and glioblastoma U-87 cells. **c** Downregulation of the Hes-1 protein in different cell lines after 72 h of treatment with SNALP miR-199b-5p and SNALP scramble in colon cancer CaCo-2, SW480, and HT-29 cells; breast cancer MCF-7 and MDA-MB231T cells; prostate cancer PC-3 cells; glioblastoma U-87 cells; and MB ONS-76, Daoy and UW-228 cells. **d** Densitometry of Hes-1 protein expression in all of the cell lines at 72 h. The normalized data were obtained from the ratio of the densitometry Hes-1 protein values between the cells treated with SNALP miR-199b-5p and with SNALP scramble

lower protein band in Supplementary Fig. 2c), which was visible in almost all of the cell lines investigated here, except for the SW480 and MCF-7 cells. This is due to the specific antibodies used here for this assay (see "Material and methods"). Our previous study showed the regulation of *Hes-1* mRNA stability by miR-199b-5p (Garzia et al. 2009). Here, we used Syber qRT-PCR to investigate whether treatment with 50 μg/ml SNALP miR-199b-5p affects *Hes-1* mRNA levels due to this target regulation at the mRNA level by miR-199b-5p. As shown in Fig. 2a, *Hes-1* mRNA was downregulated in all of the cell lines analyzed here (with 40 % to 80 % mRNA target inhibition at 72 h; *p* values: CaCo-2, 0.02; MCF-7, 0.03; PC-3, 0.0001; ONS-76, 0.05; Daoy, 0.01; UW-228, 0.02; MDA-MB231T, 0.003; and HT-29, 0.01), with the exception of the SW480, U-87, and ONS-76 cells (for $2^{\Delta Ct}$ values, see Supplementary Table 2). These data prompted us to evaluate the mRNA expression of the other miR-199b-5p targets that have been described in the literature for these cell lines that appeared not to be affected by the miR-199b-5p (Wang et al. 2011; Favreau et al. 2012). We, thus, evaluated mRNA expression of *DDR1*, *Hif-1α*, and *PODXL-1* in these cell lines. At the same time as that used for miR-199b-5p expression (72 h of treatment), we observed weak reductions in *DDR1* mRNA in the ONS-76, SW480, and U-87 cells (from 15 % to 20 % mRNA target inhibition), as shown in Fig. 2b. For the other gene targets analyzed here, only *PODXL-1* showed regulation in the ONS-76 cells (from 10 % to 15 % mRNA target inhibition), while the *Hif-1α* mRNA was not significantly affected by the SNALP miR-199b-5p delivery and overexpression at this analysis time in these cells (for $2^{\Delta Ct}$ values, see Supplementary Table 2). Overall, these data strengthen the effects on Hes-1 as the main target gene in the cells analyzed here at this particular time of inhibition using this SNALP delivery methodology. The data presented here also suggest that the analysis of mRNA levels cannot be used alone as the main methodology for the demonstration of downregulation of these miR-199b-5p targets.

For this reason, after the treatments, we also analyzed the regulation of Hes-1 by Western blotting (see Fig. 2c). Supplementary Fig. 3a shows densitometry analyses obtained from Western blotting data normalized according to the β-actin expression, showing the levels of Hes-1 in cells treated with SNALP miR-199b-5p (red line) and SNALP scramble (green line) for 72 h (see Supplementary Table 3). The normalized data were obtained as ratios of the densitometric Hes-1 protein values between the cells treated with SNALP miR-199b-5p and with SNALP scramble. The levels of the Hes-1 protein are additionally shown in Fig. 2d. Here, there was greater downregulation of this miR-199b-5p target only in Daoy, UW-228, and HT-29 cells at 72 h of treatment, while in the Caco-2, SW480, PC-3, U-87, ONS-76, MDA-MB-231 T, and MCF-7 cells, we can consider that the turnover of Hes-1 protein synthesis can overcome the downregulation by miR-199b-5p at 72 h of treatment (see Fig. 2d). These data suggest that after the treatment with SNALP miR-199b-5p, it is only in these cells that there is a better molar ratio of synthetic miR-199-5p and its mRNA target to allow the best downregulation of Hes-1 that can then be translated into regulation at the protein level. Taken altogether, here, we can conclude that SNALP miR-199b-5p can penetrate into these cells, which can, thus, be used as models for future in vivo applications in animal models of these cancer types.

SNALP miR-199b-5p modifies the expression levels of markers associated to cancer stem cells

Due to our previous findings that demonstrated that miR-199b-5p impairs the CSC compartment (CD133+ cells) both in vitro and in vivo in MB (Garzia et al. 2009), we also analyzed here the effects of SNALP miR-199b-5p (after 72 h of treatment) on protein markers associated to CSCs, i.e., on markers such as CD15 (Singh et al. 2004; Read et al. 2009; Ward et al. 2009; Andolfo et al. 2012), CD133 (Ieta et al. 2008; Shmelkov et al. 2008; Bertrand et al. 2012), and CD44 (Sheridan et al. 2006). We investigated CD15 and CD133 protein expression in Daoy and UW-228 cells, and also CD133 in HT-29 cells, which is known to be a better characterized CSC-associated marker in colon cancer. As shown in Fig. 3a, SNALP miR-199b-5p impaired the expression of CD133 and CD15 at 72 h in the MB cell lines (Daoy and UW-228 cells) that showed greater impairment of Hes1 protein levels. Similarly, the protein levels of CD133 in the HT-29 cells treated with 50 μg/ml SNALP miR-199b-5p were downregulated (Fig. 3a), while in these HT-29 cells, 25 μg/ml SNALP miR-199b-5p showed no differences compared to SNALP scramble (Supplementary Fig. 1b). This provides further indirect evidence of the best efficacy of delivery of SNALP miR199b-5p into these cells at 72 h, as previously shown for the evaluation of Hes-1 downregulation (see also Supplementary Fig. 1c).
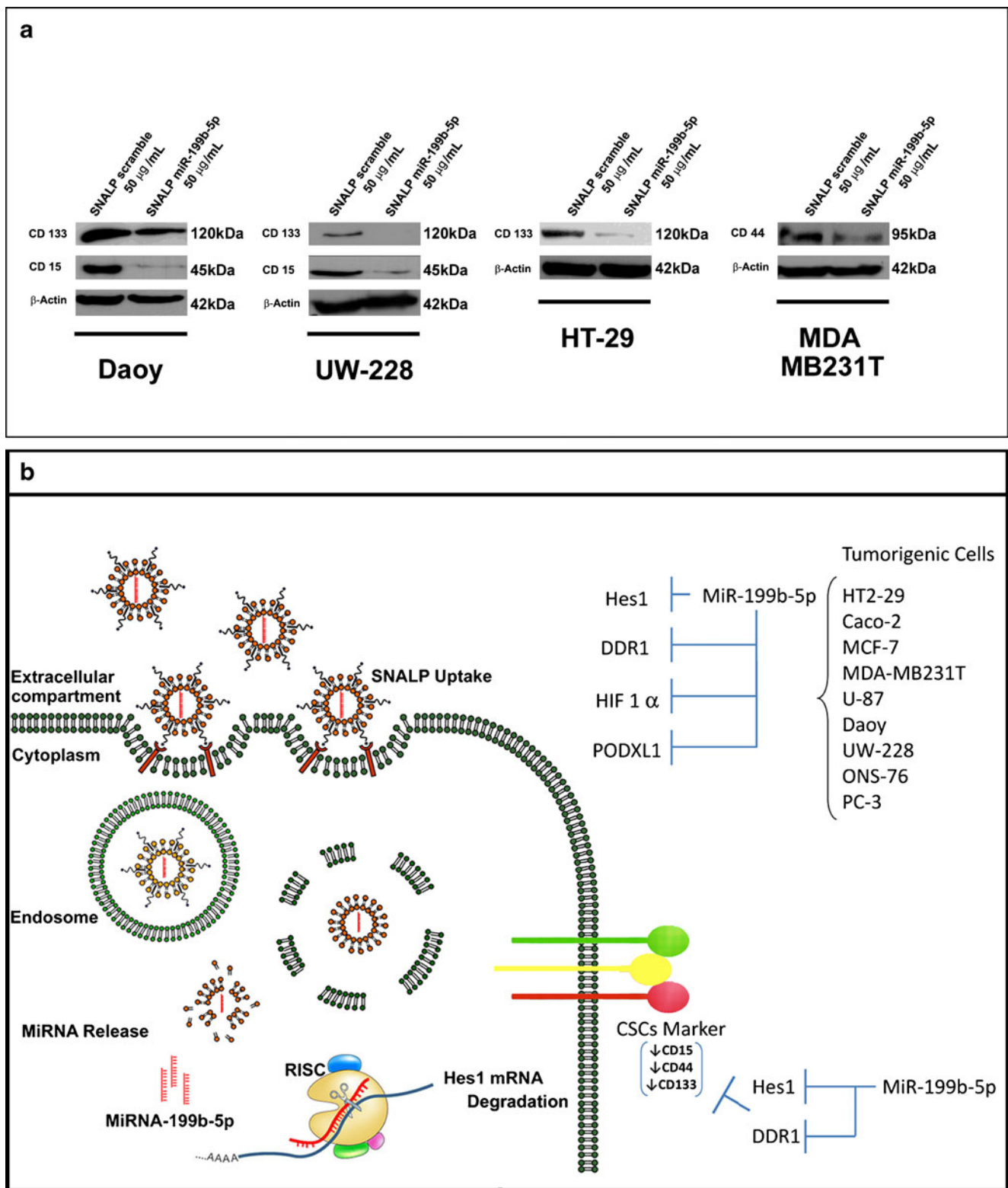
Fig. 3 Impairment of expression of cancer stem cell-associated markers in the different cell lines after miR-199b-5p delivery by SNALPs. **a** Evaluation of expression of CSC markers in different cell lines after 72 h of treatment with SNALP miR-199b-5p and SNALP scramble in colon cancer HT-29 cells, breast cancer MDA-MB231T cells, and MB Daoy and UW-228 cells. **b** Model for the impairment of CSC-associated markers by miR-199b-5p effects on its targets *Hes-1*, *PODXL-1*, *DDR1*, and *Hif-1α* in the various cell lines analyzed (as indicated)

For the evaluation of the CD44 marker, as reported by Sheridan et al., MDA-MB231T cells are known to already show high proportions of positive cells to these markers, as in particular, CD44$^+$/CD24$^-$ (98 %), as compared to MCF-7 cells that do not have these markers (see Sheridan et al. 2006). For this reason, we analyzed the effects of SNALP miR-199b-5p on CD44 in MDA-MB231T cells, and as shown in Fig. 3a, SNALP miR-199b-5p also impaired their CD44 expression.

As previously demonstrated (Garzia et al. 2009), we have confirmed here that through actions on its targets (as shown in the model in Fig. 3b), miR-199b-5p can negatively regulate the expression of markers associated with CSCs in MB and that miR-199b-5p also has a function in other tumorigenic cell lines, such as those representative of colon and breast cancers.

Discussion

MiRNAs participate in the regulation of almost every cellular process. In particular, they are useful tools for the silencing of cancers, and thus, they might act through the control of multiple target genes. We previously defined the functions of the miRNA miR-199b-5p in MB, whereby we demonstrated direct inhibition of the target Hes-1, a downstream effector of both the Notch and SHH signaling pathways. Furthermore, miR-199b-5p impairs CD133+ cells, which have been identified as markers of the CSC compartment in MB and as active agents of tumor growth in the orthotropic MB mouse model (Turner et al. 2010). We recently identified negative feedback regulation of Hes-1 through its binding to the miR-199b-5p promoter region. Additionally, we studied another target, CD15, as another marker associated with CSCs in MB (Andolfo et al. 2012). The Notch pathway has a crucial role in different tumor types. Notch signaling is known to control proliferation of stem and progenitor cells as well as cell fate specification and differentiation in the colon, and it is necessary for adenoma subtype formation in the APC mutant mouse (Katoh 2008; Reedijk et al. 2008). In breast cancer, the inhibition of Notch signaling has been shown to hinder the survival of breast CSCs (Mittal et al. 2009; Efferson et al. 2010) as well as to reverse the tumorigenic potential of breast cancer cell lines, which suggests that Notch signaling has a key role in the pathogenesis of breast cancer. In MB, the Notch/Hes-1 role remains under debate because data in the recent literature have indicated that the Notch pathway is not essential for SHH-driven MB genesis and that the maintenance of Notch signaling is not essential for initiation, engraftment, or maintenance of SHH pathway-driven MB (Hatton et al. 2010). This interpretation is supported by a study by Julian et al., where they evaluated MB formation in

the absence of RBP-J, which represents a convergence point for all of the Notch pathways (Julian et al. 2010). They showed that the canonical Notch target gene, Hes-1, is not downregulated by treatment with the Notch inhibitor MRK-003 in SmoA1 tumors. They speculated that Hes-1 is both a canonical Notch target gene and a noncanonical SHH target gene, whereas Notch1, Notch2, and Hes5 are targets of Notch signaling but not of SHH signaling. In the setting of chronic SHH pathway activation in the SmoA1 cerebellum, γ-secretase inhibitor treatments alter Notch1, Notch2, and Hes5 expression but do not affect SHH-mediated Hes-1 expression (Fouladi et al. 2011).

Targeted delivery is one of the most studied areas in cancer gene therapy. A large number of studies have demonstrated the in vivo tumor targeting of nucleic acids using nanocarriers (Judge et al. 2009). Once injected into the blood stream, stealth nanocarriers accumulate in tumors due to their enhanced permeability and retention effects. Moreover, in the case of nucleic acids, there is also the need for the use of transfection strategies that provide for their protection against degradation and promote their efficient uptake into the target cells.

Cationic liposomes are certainly the most investigated nanotechnology-based delivery system for nucleic acid delivery. However, the efficiency of these carriers can be limited by their physical instability in vivo, followed by their complexing with nucleic acids (Oh and Park 2009). SNALPs can be considered as an evolution of these cationic liposomes that can encapsulate nucleic acids into their internal aqueous cavity and thus stabilize them in biological fluids (Semple et al. 2010). Furthermore, the potential of this system for tumor targeting has been demonstrated (Leonetti et al. 2001).

In the present study, we developed a single-stranded 2′-OMe-miR-199b-5p that was loaded into SNALPs, and we have demonstrated that this synthetic miRNA has thermal stability and nuclease resistance in cells for treatments of up to 72 h, as shown by TaqMan RT-PCR.

With our treatment, we also observed different efficacies of SNALP miR-199b-5p delivery in different cell lines, which is probably linked to the variable compositions of the cell membranes and the differing abilities of these cells to internalize SNALPs; this might further be due to the different proliferation rates of these cells, which would lead to different dilution effects. To define the significant levels of these effects in the HT-29 cells, we tested two different SNALP miR-199b-5p concentrations. We further demonstrated that after 72 h of treatment, SNALP miR-199b-5p induces Hes-1 protein downregulation and impairs cell proliferation in several cell types. Here, we observed different effects on Hes-1 downregulation that might be due to variable basal levels of the Hes-1 protein in these various cell types (as shown in Supplementary Fig. 2c) and different

levels of internalization of the miR-199b-5p in these cells after SNALP miR-199b-5p treatment, thus further affecting cell proliferation. Indeed, we speculate that we have greater downregulation of Hes-1 only in Daoy, UW-228, and HT-29 cells because here we obtained better ratios of target expression and miR-199b-5p levels, such as will promote the regulation of Hes-1.

In terms of the inhibition of cell proliferation, this delivery with SNALP miR-199b-5p appears to be cell-type dependent, and this effect might be due to the other genes that are involved in the regulation of cell proliferation and direct targets of miR-199b-5p (*PODXL*, *DDR1*, and *HIF-1α*). In a study by Wang et al., for example, they suggested that miR-199b-5p negatively regulates cell growth by downregulation of hypoxia-induced HIF-1α in hepatocellular carcinoma (Wang et al. 2011). We also found that the CSCs-associated markers CD133 and CD15 (MB), CD133 (colorectal cancer cells) and CD44 (breast cancer cells) are also downregulated, suggesting that SNALP miR-199b-5p can also regulate CSC protein signaling and physiology through downregulation of the miR-199b-5p target, making this system a useful tool for in vivo application. These concepts now require further efforts for the evaluation of the effects of SNALP miR-199b-5p on CSCs properties in vivo in these hypoxic microenvironmental tumor tissues (Magee et al. 2012) where these cells reside.

The impairment of CD44 expression can be ascribed to the substantial direct inhibition of Hes-1 and its involvement in SHH-driven signaling. CD44 is not a direct target of miR-199b-5p. Indeed, Wu et al. showed a direct correlation between Hes-1 and CD44 expressions during differentiation processes in neuroepithelial cells (Wu et al. 2003). Here, we analyzed the correlation between Hes-1 and CD44 expressions in breast cancer MDA-MB231T cells as an indirect effect of Hes-1 downregulation by miR-199-5p. Moreover, as shown by Shen et al. in human hepatocellular carcinoma, deregulation of miR-199-5p is involved in malignant progression, which will further impair the ability of the cells to cross an extracellular matrix (Shen et al. 2010). The authors here speculated that miR-199b-5p can modulate cell invasion by targeting *DDR1*, a discoidin domain receptor. In addition, Kim and Nam (2006) showed that DDR1 can promote the nuclear translocation of Notch1, with regulation of its downstream pathway targets, like Hes-1. Here, we found *DDR1* mRNA downregulation in the same cell lines (SW480, U-87, and ONS76 cells) treated with SNALP miR-199b-5p. Thus, we speculate that the impaired proliferation function observed in these cell lines at this time is driven by SNALP miR-199b-5p by direct downregulation of DDR-1. Furthermore, at this time, we cannot exclude that other target genes of miR-199b-5p can influence cell proliferation, as the early events of cell proliferation (e.g., at 24 h of analysis) are most probably the early targets during the

SNALP miR-199b-5p delivery into the cells. Future studies will need to address whether the downregulation of DDR1 has a cooperative effect on the modulation of the Notch pathway and if the impairment of CSC-associated markers is due to the effects of miR-199b-5p on both of its targets (i.e., Hes-1 and DDR1), as shown in our model in Fig. 3b. Finally, here, we can conclude that SNALP miR-199b-5p and its use in the treatment of these cell lines did not show any cytotoxicity effects (see Supplemental Materials and Supplementary Fig. 3b–d), which represents a fundamental property for its eligibility as a therapeutic approach and for limiting the use of the more aggressive current therapies, such as chemotherapy agents, which can cause several and severe side effects.

Conclusions

We have provided here the basis for therapies based on the miRNA miR-199b-5p through the development of SNALPs that contain miR-199b-5p. This SNALP miR-199b-5p has high delivery efficiency and low cytotoxicity, while increasing the miR-199b-5p cellular uptake. Further studies in preclinical models are now being performed to assess the impact of off-target in vivo delivery of SNALP miR-199b-5p in different cancer types to define its efficacy and to transfer the use of SNALP miR-199b-5p to clinical trials in human.

References

Andolfo I, Liguori L, De Antonellis P, Cusanelli E, Marinaro F, Pistollato F, Garzia L, De Vita G, Petrosino G, Accordi B, Migliorati R, Basso G, Iolascon A, Cinalli G, Zollo M (2012) The micro-RNA 199b-5p regulatory circuit involves Hes1, CD15, and epigenetic modifications in medulloblastoma. Neuro-Oncology 14:596–612

Babar IA, Czochor J, Steinmetz A, Weidhaas JB, Glazer PM, Slack FJ (2011) Inhibition of hypoxia-induced miR-155 radiosensitizes hypoxic lung cancer cells. Cancer Biol Ther 12:908–914

Bertrand FE, Angus CW, Partis WJ, Sigounas G (2012) Developmental pathways in colon cancer: crosstalk between WNT, BMP, Hedgehog and Notch. Cell Cycle 11(23):4344–4351

Brennecke J, Stark A, Russell RB, Cohen SM (2005) Principles of microRNA-target recognition. PLoS Biol 3:e85

Bumcrot D, Manoharan M, Koteliansky V, Sah DW (2006) RNAi therapeutics: a potential new class of pharmaceutical drugs. Nat Chem Biol 2:711–719

Calin GA, Croce CM (2006) MicroRNA signatures in human cancers. Nat Rev Cancer 6:857–866

Calin GA, Dumitru CD, Shimizu M, Bichi R, Zupo S, Noch E, Aldler H, Rattan S, Keating M, Rai K, Rassenti L, Kipps T, Negrini M, Bullrich F, Croce CM (2002) Frequent deletions and down-regulation of micro-RNA genes miR15 and miR16 at 13q14 in chronic lymphocytic leukemia. Proc Natl Acad Sci U S A 99:15524–15529

Calin GA, Ferracin M, Cimmino A, Di Leva G, Shimizu M, Wojcik SE, Iorio MV, Visone R, Sever NI, Fabbri M, Iuliano R, Palumbo T, Pichiorri F, Roldo C, Garzon R, Sevignani C, Rassenti L, Alder H, Volinia S, Liu CG, Kipps TJ, Negrini M, Croce CM (2005) A microRNA signature associated with prognosis and progression in chronic lymphocytic leukemia. N Engl J Med 353:1793–1801

Chiu YL, Rana TM (2002) RNAi in human cells: basic structural and functional features of small interfering RNA. Mol Cell 10:549–561

Czauderna F, Fechtner M, Dames S, Aygun H, Klippel A, Pronk GJ, Giese K, Kaufmann J (2003) Structural variations and stabilising modifications of synthetic siRNAs in mammalian cells. Nucleic Acids Res 31:2705–2716

Danza G, Di Serio C, Rosati F, Lonetto G, Sturli N, Kacer D, Pennella A, Ventimiglia G, Barucci R, Piscazzi A, Prudovsky I, Landriscina M, Marchionni N, Tarantini F (2012) Notch signaling modulates hypoxia-induced neuroendocrine differentiation of human prostate cancer cells. Mol Cancer Res 10:230–238

de Antonellis P, Medaglia C, Cusanelli E, Andolfo I, Liguori L, De Vita G, Carotenuto M, Bello A, Formiggini F, Galeone A, De Rosa G, Virgilio A, Scognamiglio I, Sciro M, Basso G, Schulte JH, Cinalli G, Iolascon A, Zollo M (2011) MiR-34a targeting of Notch ligand delta-like 1 impairs CD15+/CD133+ tumor-propagating cells and supports neural differentiation in medulloblastoma. PLoS One 6:e24584

Dorsett Y, Tuschl T (2004) siRNAs: applications in functional genomics and potential as therapeutics. Nat Rev Drug Discov 3:318–329

Efferson CL, Winkelmann CT, Ware C, Sullivan T, Giampaoli S, Tammam J, Patel S, Mesiti G, Reilly JF, Gibson RE, Buser C, Yeatman T, Coppola D, Winter C, Clark EA, Draetta GF, Strack PR, Majumder PK (2010) Downregulation of Notch pathway by a gamma-secretase inhibitor attenuates AKT/mammalian target of rapamycin signaling and glucose uptake in an ERBB2 transgenic breast cancer model. Cancer Res 70:2476–2484

Esquela-Kerscher A, Slack FJ (2006) Oncomirs—microRNAs with a role in cancer. Nat Rev Cancer 6:259–269

Fabian MR, Sonenberg N (2012) The mechanics of miRNA-mediated gene silencing: a look under the hood of miRISC. Nat Struct Mol Biol 19:586–593

Favreau AJ, Cross EL, Sathyanarayana P (2012) miR-199b-5p directly targets PODXL and DDR1 and decreased levels of miR-199b-5p correlate with elevated expressions of PODXL and DDR1 in acute myeloid leukemia. Am J Hematol 87:442–446

Fouladi M, Stewart CF, Olson J, Wagner LM, Onar-Thomas A, Kocak M, Packer RJ, Goldman S, Gururangan S, Gajjar A, Demuth T, Kun LE, Boyett JM, Gilbertson RJ (2011) Phase I trial of MK-0752 in children with refractory CNS malignancies: a pediatric brain tumor consortium study. J Clin Oncol 29:3529–3534

Frank-Kamenetsky M, Grefhorst A, Anderson NN, Racie TS, Bramlage B, Akinc A, Butler D, Charisse K, Dorkin R, Fan Y, Gamba-Vitalo C, Hadwiger P, Jayaraman M, John M, Jayaprakash KN, Maier M, Nechev L, Rajeev KG, Read T, Rohl I, Soutschek J, Tan P, Wong J, Wang G, Zimmermann T, de Fougerolles A, Vornlocher HP, Langer R, Anderson DG, Manoharan M, Koteliansky V, Horton JD, Fitzgerald K (2008) Therapeutic RNAi targeting PCSK9 acutely lowers plasma cholesterol in rodents and LDL cholesterol in nonhuman primates. Proc Natl Acad Sci U S A 105:11915–11920

Garzia L, Andolfo I, Cusanelli E, Marino N, Petrosino G, De Martino D, Esposito V, Galeone A, Navas L, Esposito S, Gargiulo S, Fattet S, Donofrio V, Cinalli G, Brunetti A, Vecchio LD, Northcott PA, Delattre O, Taylor MD, Iolascon A, Zollo M (2009) MicroRNA-199b-5p impairs cancer stem cells through negative regulation of HES1 in medulloblastoma. PLoS One 4:e4998

Garzon R, Calin GA, Croce CM (2009) MicroRNAs in Cancer. Annu Rev Med 60:167–179

Gaur A, Jewell DA, Liang Y, Ridzon D, Moore JH, Chen C, Ambros VR, Israel MA (2007) Characterization of microRNA expression levels and their biological correlates in human cancer cell lines. Cancer Res 67:2456–2468

Gomes-da-Silva LC, Fonseca NA, Moura V, Pedroso de Lima MC, Simoes S, Moreira JN (2012) Lipid-based nanoparticles for siRNA delivery in cancer therapy: paradigms and challenges. Acc Chem Res 45:1163–1171

Gursel DB, Berry N, Boockvar JA (2012) The contribution of Notch signaling to glioblastoma via activation of cancer stem cell self-renewal: the role of the endothelial network. Neurosurgery 70: N19–N21

Hatton BA, Villavicencio EH, Pritchard J, LeBlanc M, Hansen S, Ulrich M, Ditzler S, Pullar B, Stroud MR, Olson JM (2010) Notch signaling is not essential in sonic hedgehog-activated medulloblastoma. Oncogene 29:3865–3872

He L, He X, Lim LP, de Stanchina E, Xuan Z, Liang Y, Xue W, Zender L, Magnus J, Ridzon D, Jackson AL, Linsley PS, Chen C, Lowe SW, Cleary MA, Hannon GJ (2007) A microRNA component of the p53 tumour suppressor network. Nature 447:1130–1134

Heinrich EM, Dimmeler S (2012) MicroRNAs and stem cells: control of pluripotency, reprogramming, and lineage commitment. Circ Res 110:1014–1022

Ieta K, Tanaka F, Haraguchi N, Kita Y, Sakashita H, Mimori K, Matsumoto T, Inoue H, Kuwano H, Mori M (2008) Biological and genetic characteristics of tumor-initiating cells in colon cancer. Ann Surg Oncol 15:638–648

Ingram WJ, McCue KI, Tran TH, Hallahan AR, Wainwright BJ (2008) Sonic Hedgehog regulates Hes1 through a novel mechanism that is independent of canonical Notch pathway signalling. Oncogene 27:1489–1500

Jores K, Haberland A, Wartewig S, Mader K, Mehnert W (2005) Solid lipid nanoparticles (SLN) and oil-loaded SLN studied by spectrofluorometry and Raman spectroscopy. Pharm Res 22:1887–1897

Judge AD, Bola G, Lee AC, MacLachlan I (2006) Design of noninflammatory synthetic siRNA mediating potent gene silencing in vivo. Mol Ther 13:494–505

Judge AD, Robbins M, Tavakoli I, Levi J, Hu L, Fronda A, Ambegia E, McClintock K, MacLachlan I (2009) Confirming the RNAi-mediated mechanism of action of siRNA-based cancer therapeutics in mice. J Clin Investig 119:661–673

Julian E, Dave RK, Robson JP, Hallahan AR, Wainwright BJ (2010) Canonical Notch signaling is not required for the growth of Hedgehog pathway-induced medulloblastoma. Oncogene 29:3465–3476

Katoh M (2008) WNT signaling in stem cell biology and regenerative medicine. Curr Drug Targets 9:565–570

Katoh M, Katoh M (2007) Notch signaling in gastrointestinal tract (review). Int J Oncol 30:247–251

Kim VN, Nam JW (2006) Genomics of microRNA. Trends Genet 22:165–173

Leonetti C, Biroccio A, Benassi B, Stringaro A, Stoppacciaro A, Semple SC, Zupi G (2001) Encapsulation of c-myc antisense oligodeoxynucleotides in lipid particles improves antitumoral efficacy in vivo in a human melanoma line. Cancer Gene Ther 8:459–468

Livak KJ, Schmittgen TD (2001) Analysis of relative gene expression data using real-time quantitative PCR and the 2(−delta delta C(T)) Method. Methods 25:402–408

Magee JA, Piskounova E, Morrison SJ (2012) Cancer stem cells: impact, heterogeneity, and uncertainty. Cancer Cell 21(3):283–296

Martins S, Costa-Lima S, Carneiro T, Cordeiro-da-Silva A, Souto EB, Ferreira DC (2012) Solid lipid nanoparticles as intracellular drug transporters: an investigation of the uptake mechanism and pathway. Int J Pharm 430:216–227

Meister G, Tuschl T (2004) Mechanisms of gene silencing by double-stranded RNA. Nature 431:343–349

Mittal S, Subramanyam D, Dey D, Kumar RV, Rangarajan A (2009) Cooperation of Notch and Ras/MAPK signaling pathways in human breast carcinogenesis. Mol Cancer 8:128

Moreira JN, Santos A, Moura V, Pedroso de Lima MC, Simoes S (2008) Non-viral lipid-based nanoparticles for targeted cancer systemic gene silencing. J Nanosci Nanotechnol 8:2187–2204

Morrissey DV, Lockridge JA, Shaw L, Blanchard K, Jensen K, Breen W, Hartsough K, Machemer L, Radka S, Jadhav V, Vaish N, Zinnen S, Vargeese C, Bowman K, Shaffer CS, Jeffs LB, Judge A, MacLachlan I, Polisky B (2005) Potent and persistent in vivo anti-HBV activity of chemically modified siRNAs. Nat Biotechnol 23:1002–1007

Morton JP, Lewis BC (2007) Shh signaling and pancreatic cancer: implications for therapy? Cell Cycle 6:1553–1557

Nana-Sinkam SP, Croce CM (2011) Non-coding RNAs in cancer initiation and progression and as novel biomarkers. Mol Oncol 5:483–491

Oh YK, Park TG (2009) siRNA delivery systems for cancer treatment. Adv Drug Deliv Rev 61:850–862

Puri A, Loomis K, Smith B, Lee JH, Yavlovich A, Heldman E, Blumenthal R (2009) Lipid-based nanoparticles as pharmaceutical drug carriers: from concepts to clinic. Crit Rev Ther Drug Carrier Syst 26:523–580

Read TA, Fogarty MP, Markant SL, McLendon RE, Wei Z, Ellison DW, Febbo PG, Wechsler-Reya RJ (2009) Identification of CD15 as a marker for tumor-propagating cells in a mouse model of medulloblastoma. Cancer Cell 15:135–147

Reedijk M, Odorcic S, Zhang H, Chetty R, Tennert C, Dickson BC, Lockwood G, Gallinger S, Egan SE (2008) Activation of Notch signaling in human colon adenocarcinoma. Int J Oncol 33:1223–1229

Robbins M, Judge A, MacLachlan I (2009) siRNA and innate immunity. Oligonucleotides 19:89–102

Schoof CR, Botelho EL, Izzotti A, Vasques Ldos R (2012) MicroRNAs in cancer treatment and prognosis. Am J Cancer Res 2:414–433

Schreck KC, Taylor P, Marchionni L, Gopalakrishnan V, Bar EE, Gaiano N, Eberhart CG (2010) The Notch target Hes1 directly modulates Gli1 expression and Hedgehog signaling: a potential mechanism of therapeutic resistance. Clin Cancer Res 16:6060–6070

Semple SC, Akinc A, Chen J, Sandhu AP, Mui BL, Cho CK, Sah DW, Stebbing D, Crosley EJ, Yaworski E, Hafez IM, Dorkin JR, Qin J, Lam K, Rajeev KG, Wong KF, Jeffs LB, Nechev L, Eisenhardt ML, Jayaraman M, Kazem M, Maier MA, Srinivasulu M, Weinstein MJ, Chen Q, Alvarez R, Barros SA, De S, Klimuk SK, Borland T, Kosovrasti V, Cantley WL, Tam YK, Manoharan M, Ciufolini MA, Tracy MA, de Fougerolles A, MacLachlan I, Cullis PR, Madden TD, Hope MJ (2010) Rational design of cationic lipids for siRNA delivery. Nat Biotechnol 28:172–176

Shen Q, Cicinnati VR, Zhang X, Iacob S, Weber F, Sotiropoulos GC, Radtke A, Lu M, Paul A, Gerken G, Beckebaum S (2010) Role of microRNA-199a-5p and discoidin domain receptor 1 in human hepatocellular carcinoma invasion. Mol Cancer 9:227

Sheridan C, Kishimoto H, Fuchs RK, Mehrotra S, Bhat-Nakshatri P, Turner CH, Goulet R Jr, Badve S, Nakshatri H (2006) CD44+/CD24− breast cancer cells exhibit enhanced invasive properties: an early step necessary for metastasis. Breast Cancer Res 8:R59

Shimizu T, Kagawa T, Inoue T, Nonaka A, Takada S, Aburatani H, Taga T (2008) Stabilized beta-catenin functions through TCF/LEF proteins and the Notch/RBP-Jkappa complex to promote proliferation and suppress differentiation of neural precursor cells. Mol Cell Biol 28:7427–7441

Shmelkov SV, Butler JM, Hooper AT, Hormigo A, Kushner J, Milde T, St Clair R, Baljevic M, White I, Jin DK, Chadburn A, Murphy AJ, Valenzuela DM, Gale NW, Thurston G, Yancopoulos GD, D'Angelica M, Kemeny N, Lyden D, Rafii S (2008) CD133 expression is not restricted to stem cells, and both CD133+ and CD133− metastatic colon cancer cells initiate tumors. J Clin Investig 118:2111–2120

Simoes S, Filipe A, Faneca H, Mano M, Penacho N, Duzgunes N, de Lima MP (2005) Cationic liposomes for gene delivery. Expert Opin Drug Deliv 2:237–254

Singh SK, Hawkins C, Clarke ID, Squire JA, Bayani J, Hide T, Henkelman RM, Cusimano MD, Dirks PB (2004) Identification of human brain tumour initiating cells. Nature 432:396–401

Takahashi M, Nagai C, Hatakeyama H, Minakawa N, Harashima H, Matsuda A (2012) Intracellular stability of 2′-OMe-4′-thioribonucleoside modified siRNA leads to long-term RNAi effect. Nucleic Acids Res 40:5787–5793

Turner JD, Williamson R, Almefty KK, Nakaji P, Porter R, Tse V, Kalani MY (2010) The many roles of microRNAs in brain tumor biology. Neurosurg Focus 28: E3

Wang C, Song B, Song W, Liu J, Sun A, Wu D, Yu H, Lian J, Chen L, Han J (2011) Underexpressed microRNA-199b-5p targets hypoxia-inducible factor-1alpha in hepatocellular carcinoma and predicts prognosis of hepatocellular carcinoma patients. J Gastroenterol Hepatol 26:1630–1637

Ward M, Guntert A, Campbell J, Pike I (2009) Proteomics for brain disorders—the promise for biomarkers. Ann N Y Acad Sci 1180:68–74

Watts JK, Deleavey GF, Damha MJ (2008) Chemically modified siRNA: tools and applications. Drug Discov Today 13:842–855

Whitehead KA, Langer R, Anderson DG (2009) Knocking down barriers: advances in siRNA delivery. Nat Rev Drug Discov 8:129–138

Wu Y, Liu Y, Levine EM, Rao MS (2003) Hes1 but not Hes5 regulates an astrocyte versus oligodendrocyte fate choice in glial restricted precursors. Dev Dyn 226:675–689

Yang XZ, Dou S, Sun TM, Mao CQ, Wang HX, Wang J (2011) Systemic delivery of siRNA with cationic lipid assisted PEG-PLA nanoparticles for cancer therapy. J Control Release 156:203–211

Zhang B, Pan X, Cobb GP, Anderson TA (2007) microRNAs as oncogenes and tumor suppressors. Dev Biol 302:1–12

Zhao L, Chen X, Cao Y (2011) New role of microRNA: carcinogenesis and clinical application in cancer. Acta Biochim Biophys Sin (Shanghai) 43:831–839

Zimmermann TS, Lee AC, Akinc A, Bramlage B, Bumcrot D, Fedoruk MN, Harborth J, Heyes JA, Jeffs LB, John M, Judge AD, Lam K, McClintock K, Nechev LV, Palmer LR, Racie T, Rohl I, Seiffert S, Shanmugam S, Sood V, Soutschek J, Toudjarska I, Wheat AJ, Yaworski E, Zedalis W, Koteliansky V, Manoharan M, Vornlocher HP, MacLachlan I (2006) RNAi-mediated gene silencing in non-human primates. Nature 441:111–114